Springer

Available online at https://link.springer.com
http://www.jhydrod.com/
2018,30(3):453-462
https://doi.org/10.1007/s42241-018-0041-6

Waves propagating over a two-layer porous barrier on a seabed *

Qiang Lin [1,2] (林强), Qing-rui Meng [3,4] (孟庆瑞), Dong-qiang Lu [3,4] (卢东强)
1. *China Ship Scientific Research Center, Wuxi 214082, China*
2. *Shanghai Oriental Maritime Engineering Technology Company Limited, Shanghai 200011, China*
3. *Shanghai Institute of Applied Mathematics and Mechanics, Shanghai University, Shanghai 200072, China*
4. *Shanghai Key Laboratory of Mechanics in Energy Engineering, Shanghai 200072, China*

(Received February 22, 2017, Accepted August 15, 2017)

Abstract: A research of wave propagation over a two-layer porous barrier, each layer of which is with different values of porosity and friction, is conducted with a theoretical model in the frame of linear potential flow theory. The model is more appropriate when the seabed consists of two different properties, such as rocks and breakwaters. It is assumed that the fluid is inviscid and incompressible and the motion is irrotational. The wave numbers in the porous region are complex ones, which are related to the decaying and propagating behaviors of wave modes. With the aid of the eigenfunction expansions, a new inner product of the eigenfunctions in the two-layer porous region is proposed to simplify the calculation. The eigenfunctions, under this new definition, possess the orthogonality from which the expansion coefficients can be easily deduced. Selecting the optimum truncation of the series, we derive a closed system of simultaneous linear equations for the same number of the unknown reflection and transmission coefficients. The effects of several physical parameters, including the porosity, friction, width, and depth of the porous barrier, on the dispersion relation, reflection and transmission coefficients are discussed in detail through the graphical representations of the solutions. It is concluded that these parameters have certain impacts on the reflection and transmission energy.

Key words: Two-layer porous barrier, inner product, matched eigenfunction expansions

Introduction

The interactions between waves and porous regions have given rise to extensive attention among costal engineering designers. The porous media are probably rocks and breakwaters, which may reflect the energy by adopting the proper porosity and dissipate the energy by friction. The study on the interactions between waves and porous regions is useful to analyze the wave motion and wave loads on the marine structures. For instance, the bottoms of permeable breakwaters are stuck on the seabed, while their tops are below or pierce the water. The porous breakwaters may play a significant role in reducing the total load on the structures.

When the waves encounter the porous structures, some energy is reflected into the open water; some is transmitted into the porous region, the others dissipated. The specific amount of each part depends on the parameters of the porous media. Sollitt and Cross[1] proposed a theory to predict the reflected and transmitted energy of a rectangular breakwater with the matching conditions at the windward and leeward faces. With a similar model, Chwang[2] developed a porous-wavemaker theory to analyze the small amplitude surface waves generated by the horizontal oscillations of a porous vertical plate. The effects of two important parameters, namely the wave-effect and the porous-effect parameters, on the surface waves and hydrodynamic pressures were analyzed in detail. Sahoo et al.[3] extended this work to four different configurations: a bottom-standing barrier, a surface-piercing barrier, a barrier with a gap, and a submerged barrier, in the case of obliquely incident surface waves. A new model of a vertical porous structure placed near and away from a rigid vertical wall was studied

* Project supported by the Ministry of Industry and Information Technology (MIIT) with the Research Project in the Fields of High-Technology Ships (Grant Nos. [2016]22, [2016]548), the National Natural Science Foundation of China (Grant No. 11472166) and the Natural Science Foundation of Jiangsu Province (Grant No. BK20130109).
Biography: Qiang Lin (1990-), Male, Master,
E-mail: linqiang@702sh.com
Corresponding author: Dong-qiang Lu,
E-mail: dqlu@shu.edu.cn

by Das and Bora[4] within the framework of linear water wave theory. Zhao et al.[5] considered the wave interaction with a vertical wall protected by a submerged porous bar and claimed that the wave run-up and wave force were effectively reduced by the porous bar. In order to verify the theoretical method, some experiments were carried out by Zhang et al.[6] and Zhai et al.[7] in wave flumes to measure the pore pressure.

For an impermeable seabed, free surface waves consist of the propagating and evanescent waves. As for the waves in the porous region, the wave numbers become complex ones, which was detailedly analyzed by Jeng[8]. The real part is related to the wavelength, while the imaginary part is the damping of the water waves. Metallinos et al.[9] investigated the submerged porous breakwaters of mild to steep slopes with theoretical and experimental methods. Mohapatra[10] presented an expression of Green's function suitable for the scattering problem with obliquely incident waves propagating over a region, in which the upper surface was covered by an infinitely extended thin elastic plate and the lower surface was a porous bottom with a small deformation. The influences of poroelastic bed on flexural-gravity waves in both cases of single-layer and two-layer fluids were studied by Das et al.[11] which revealed that the phase speed for the flexural-gravity mode in the two-layer fluid reaches the maximum value for large porosities when the interface is close to the poroelastic bed. With a numerical model, Shoushtari and Cartwright[12] analyzed the effects of porous medium deformation on the dispersion of water-table waves.

In real circumstances, ocean waves are usually simultaneously accompanied by currents. Based on Biot's poroelastic dynamic theory, Ye and Jeng[13] investigated the model of seabed response with waves and currents. Furthermore, Zhang et al.[14] had a parametric study for the influence of the currents and non-linear waves on the seabed responses. A numerical calculation model was proposed by Zhang et al.[15] to analyze the stability of seabed under wave and current loadings. It has shown that the excess pore pressure increases with increasing flow velocity.

A porous model of different parameters is more appropriate when the seabed consists of multiple-layer breakwater and rocks. Seymour et al.[16] proposed a new method for the wave-induced response in a soil matrix, with the permeability as a function of depth. Jeng and Seymour[17] verified an analytical solution of soil response with variable permeability by a comparison with the conventional solution for uniform permeability. A stochastic finite element model was put forward to study the wave-induced seabed response in a spatially random porous seabed by Zhang et al.[18].

1. Mathematical formulation

The Cartesian coordinates are chosen in such a way that $z=0$ coincides with the undisturbed upper surface. The x axis points horizontally rightwards and the z axis points vertically upwards, with $z=-H$ as the flat bottom, as shown in Fig. 1. With the assumptions that the fluids are inviscid and incompressible and that the motion is irrotational, the problem can be described by the potential flow theory. The whole flow domain is mathematically divided into three parts, an open water region Ω_1 $(-\infty<x<-b)$, a porous water region Ω_2 $(-b<x<b)$ with a two-layer porous barrier mounted on seabed, and an open water region Ω_3 $(b<x<\infty)$. In the porous water region Ω_2, h_0, h_1 and h_2 are the depths of the pure water region, and the first-layer and the second-layer porous water, respectively, where $h_0+h_1+h_2=H$.

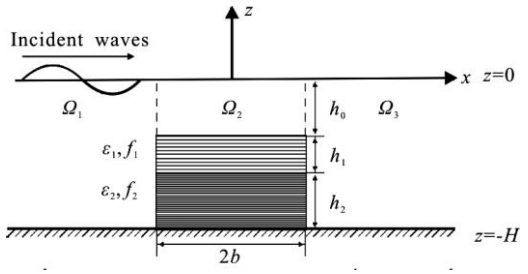

Fig. 1 Schematic diagram for waves propagation over a two-layer porous barrier on a seabed

Assuming that the incident waves are simply time-harmonic with a given angular frequency ω, we have, via separating the time factor, the velocity potential $\mathrm{Re}[\Phi(x,z)\mathrm{e}^{-\mathrm{i}\omega t}]$, the surface elevation $\mathrm{Re}[\zeta(x,z)\mathrm{e}^{-\mathrm{i}\omega t}]$, $\zeta(x)$ are the spatial elevations on the surface $z=0$ and t is the time variable. The spatial velocity potential $\Phi(x,z)$ satisfies the Laplace equation

$$\left(\frac{\partial^2}{\partial x^2}+\frac{\partial^2}{\partial z^2}\right)\Phi=0 \quad (-\infty<x<\infty,\ -H<z<0) \tag{1}$$

The boundary conditions on the free surface, in combination of the kinematic and dynamic conditions, can be formulated as

$$g\frac{\partial\Phi}{\partial z}-\omega^2\Phi=0 \quad (-\infty<x<\infty,\ z=0) \tag{2}$$

where g is the gravitational acceleration.

The bottom boundary condition of the flat rigid

seabed reads

$$\frac{\partial \Phi}{\partial z}=0 \quad (-\infty<x<\infty,\ \ z=-H) \tag{3}$$

The velocity and pressure must be continuous at the interface between media for different layers, respectively. Three dimensionless physical parameters of the porous media, i.e., the porosity ε, the linear friction factor f and the inertial term s, are introduced by Sollitt and Cross[1]. The continuous conditions at the interface are written as, for $-b<x<b$,

$$\frac{\partial \Phi_0}{\partial z}=\varepsilon_1\frac{\partial \Phi_1}{\partial z} \quad (z=-h_0) \tag{4}$$

$$\Phi_0=G_1\Phi_1 \quad (z=-h_0) \tag{5}$$

$$\varepsilon_1\frac{\partial \Phi_1}{\partial z}=\varepsilon_2\frac{\partial \Phi_2}{\partial z} \quad (z=-h_0-h_1) \tag{6}$$

$$G_1\Phi_1=G_2\Phi_2 \quad (z=-h_0-h_1) \tag{7}$$

where $\Phi_m(x,z)$ with $m=0,1,2$ are the spatial velocity potentials of the pure water $(m=0)$, the first layer porous region $(m=1)$ and the second layer porous region $(m=2)$ in Ω_2, ε_m with $m=0,1,2$ are the porosity of the pure water $(m=0)$, the first layer porous region $(m=1)$ and the second layer porous region $(m=2)$, G_m with $m=0,1,2$ is calculated from s_m+if_m, s_m and f_m are the inertial term and the linear friction factor of the first layer porous region $(m=1)$ and the second layer porous region $(m=2)$ while $s_0=1$ and $f_0=1$ represent those for the pure water.

The matching relations of the pressure and the velocity on the interface $x=\pm b$ between the open water region (Ω_1,Ω_3) and the porous water region Ω_2 are presented via the following equations:

$$\Phi(x,z)\big|_{x=-b^-}=G_m\Phi_m(x,z)\big|_{x=-b^+} \quad (x=-b) \tag{8}$$

$$\left.\frac{\partial \Phi(x,z)}{\partial x}\right|_{x=-b^-}=\varepsilon_m\left.\frac{\partial \Phi_m(x,z)}{\partial x}\right|_{x=-b^+} \quad (x=-b) \tag{9}$$

$$\Phi(x,z)\big|_{x=b^+}=G_m\Phi_m(x,z)\big|_{x=b^-} \quad (x=b) \tag{10}$$

$$\left.\frac{\partial \Phi(x,z)}{\partial x}\right|_{x=b^+}=\varepsilon_m\left.\frac{\partial \Phi_m(x,z)}{\partial x}\right|_{x=b^-} \quad (x=b) \tag{11}$$

for $-H<z<0$ and $m=0,1,2$.

2. Method of solution

2.1 *Dispersion relations*

It is well known that the dispersion relation for the pure water in the regions Ω_1 and Ω_3 can be easily obtained as follows

$$\omega^2=gk\tanh(kH) \tag{12}$$

where k is the wave number. For a given frequency ω, the dispersion relation Eq. (12) for the open water region yields one positive real root k_0, and has an infinite number of imaginary roots $\mathrm{i}k_i\ (i=1,2,\cdots)$, where k_i is positive and real. The real root corresponds to the propagating wave modes in the open water region and the imaginary roots $\mathrm{i}k_i$ correspond to the evanescent modes in the open water region.

With the help of the general solutions of Eq. (1) consisting of $\mathrm{e}^{\mathrm{i}\tilde{k}x+\tilde{k}z}$, where $\tilde{k}$ is the wave number of the porous region, the dispersion relation for the porous region can be derived by solving simultaneously Eqs. (2)-(7), which is formulated as

$$\omega^2=\frac{g\tilde{k}(G_1\gamma_2t_0+\varepsilon_1\gamma_1t_2+\varepsilon_1\gamma_2t_1+G_1\gamma_1t_0t_1t_2)}{G_1\gamma_2+G_1\gamma_1t_1t_2+\varepsilon_1\gamma_2t_0t_1+\varepsilon_1\gamma_1t_0t_2} \tag{13}$$

where $t_0=\tanh\tilde{k}h_0$, $t_1=\tanh\tilde{k}h_1$, $t_2=\tanh\tilde{k}h_2$, $\gamma_1=G_1/G_2$ and $\gamma_2=\varepsilon_1/\varepsilon_2$. In accordance with the expressions, γ_1 is a complex number while γ_2 is a positive real number. Only when $s_1/s_2=f_1/f_2$, γ_1 reduces to a positive one.

As the value of the depth h_2 tends to zero, t_2 tends to zero and γ_1 and γ_2 tend to 1.

The equation then reduces to the expression

$$\omega^2=\frac{g\tilde{k}(G_1t_0+\varepsilon_1t_1)}{G_1+\varepsilon_1t_0t_1} \tag{14}$$

which is the same as the equation derived by Meng and Lu[19]. When h_1 tends to zero and t_1 tends to zero, the above equation reduces to the expression

$$\omega^2=g\tilde{k}t_0 \tag{15}$$

which is similar to Eq. (12).

From Eq. (13), we can obtain, for a given ω

and $f=0$, one positive real roots and an infinite number of imaginary roots. For a non-zero linear friction factor f, the equation will have an infinite number of complex roots $\tilde{k}_j=\tilde{\alpha}_j+\mathrm{i}\tilde{\beta}_j$, where $\tilde{\alpha}_j$ and $\tilde{\beta}_j$ with $(j=0,1,2,3\cdots)$ are real numbers, which are associated with the decaying propagating wave modes in the porous region. Among $\tilde{k}_j$ $(j=0,1,2,3\cdots)$, the waves corresponding to $\tilde{k}_0$ have the smallest wavelength and decaying rate.

2.2 *Expression for the spatial velocity potential*

The plane incident waves from the negative infinity in the Cartesian coordinates are denoted by $\zeta_0\mathrm{e}^{\mathrm{i}kx}$, where ζ_0 is the wave amplitude. The velocity potentials referring to the open water region Ω_1 $(-\infty<x<-b)$, the porous water region Ω_2 $(-b<x<b)$ and the open water region Ω_3 $(b<x<\infty)$ are marked with Φ_{Ω_1}, Φ_{Ω_2} and Φ_{Ω_3}, respectively. With the method of separation of variables, the velocity potentials Φ_{Ω_1}, Φ_{Ω_2} and Φ_{Ω_3} can be formulated by

$$\Phi_{\Omega_1}=I_0\mathrm{e}^{\mathrm{i}k_0x}Z_0(z)+R_0\mathrm{e}^{-\mathrm{i}k_0x}Z_0(z)+\sum_{i=1}^{\infty}R_i\mathrm{e}^{k_ix}Z_i(z) \quad (16)$$

$$\Phi_{\Omega_2}=\sum_{j=0}^{\infty}(\tilde{T}_j\mathrm{e}^{\mathrm{i}\tilde{k}_jx}+\tilde{R}_j\mathrm{e}^{-\mathrm{i}\tilde{k}_jx})\tilde{Z}_j(z) \quad (17)$$

$$\Phi_{\Omega_3}=T_0\mathrm{e}^{\mathrm{i}k_0x}Z_0(z)+\sum_{i=1}^{\infty}T_i\mathrm{e}^{-k_ix}Z_i(z) \quad (18)$$

where

$$I_0=-\mathrm{i}\omega\zeta_0\left[\frac{\partial Z(k_0,z)}{\partial z}\right]_{z=0}^{-1} \quad (19)$$

$$\{Z_0(z),Z_i(z),\tilde{Z}_j(z)\}=\{U(k_0,z),U(\mathrm{i}k_i,z),V(\tilde{k}_j,z)\}$$

$$(i=1,2,\cdots,\ j=1,2,\cdots) \quad (20)$$

$$U(k,z)=\frac{\cosh k(z+H)}{\cosh kH} \quad (-H\le z\le 0) \quad (21)$$

$$V(\tilde{k},z)=\frac{1}{\cosh\tilde{k}H}\Big[G_1\cosh\tilde{k}(h_0+z)\cdot$$

$$\left(\frac{1}{\gamma_1}\cosh\tilde{k}h_1\cosh\tilde{k}h_2+\frac{1}{\gamma_2}\sinh\tilde{k}h_1\sinh\tilde{k}h_2\right)+$$

$$\varepsilon_1\sinh\tilde{k}(h_0+z)\left(\frac{1}{\gamma_1}\sinh\tilde{k}h_1\cosh\tilde{k}h_2+\right.$$

$$\left.\frac{1}{\gamma_2}\cosh\tilde{k}h_1\sinh\tilde{k}h_2\right)\Big] \quad (-h_0\le z\le 0) \quad (22a)$$

$$V(\tilde{k},z)=\frac{1}{\cosh\tilde{k}H}\left[\frac{1}{\gamma_1}\cosh\tilde{k}h_2\cosh\tilde{k}(h_0+h_1+z)+\right.$$

$$\left.\frac{1}{\gamma_2}\sinh\tilde{k}h_2\sinh\tilde{k}(h_0+h_1+z)\right] \quad (22b)$$

$$V(\tilde{k},z)=\frac{\cosh\tilde{k}(z+H)}{\cosh\tilde{k}H} \quad (-H\le z<-h_0-h_1) \quad (22c)$$

where $U(k,z)$ and $V(\tilde{k},z)$ are the vertical eigenfunctions of the open water region and porous regions, respectively, the reflection coefficients R_0 and R_i, the transmission coefficients T_0 and T_i, and the intermediate variables $\tilde{R}_j$ and $\tilde{T}_j$ are complex numbers to be determined, where $i=1,2,\cdots$ and $j=0,1,2,\cdots$, $\sum_i$ and $\sum_j$ are the summation symbols corresponding to $i=1,2,\cdots$ and $j=0,1,2,\cdots$, respectively.

2.3 *Solutions for the reection and transmission coefficients*

The core process is to solve unknown expansion coefficients from the series equations. Substituting Φ_{Ω_1}, Φ_{Ω_2} and Φ_{Ω_3} in Eqs. (16)-(18) into the matching conditions Eqs. (8)-(11) for the interface at $x=\pm b$, we obtain, for $m=0,1,2$,

$$I_0\mathrm{e}^{-\mathrm{i}bk_0}Z_0(z)+R_0\mathrm{e}^{\mathrm{i}bk_0}Z_0(z)+\sum_{i=1}^{\infty}R_i\mathrm{e}^{-bk_i}Z_i(z)=$$

$$\sum_{j=0}^{\infty}G_m(\tilde{T}_j\mathrm{e}^{-\mathrm{i}b\tilde{k}_j}+\tilde{R}_j\mathrm{e}^{\mathrm{i}b\tilde{k}_j})\tilde{Z}_j(z) \quad (x=-b) \quad (23)$$

$$\mathrm{i}k_0I_0\mathrm{e}^{-\mathrm{i}bk_0}Z_0(z)-\mathrm{i}k_0R_0\mathrm{e}^{\mathrm{i}bk_0}Z_0(z)+\sum_{i=1}^{\infty}k_iR_i\mathrm{e}^{-bk_i}Z_i(z)=$$

$$\sum_{j=0}^{\infty}\mathrm{i}\tilde{k}_j\varepsilon_m(\tilde{T}_j\mathrm{e}^{-\mathrm{i}b\tilde{k}_j}-\tilde{R}_j\mathrm{e}^{\mathrm{i}b\tilde{k}_j})\tilde{Z}_j(z) \quad (x=-b) \quad (24)$$

$$\sum_{j=0}^{\infty} G_m(\tilde{T}_j e^{ib\tilde{k}_j} + \tilde{R}_j e^{-ib\tilde{k}_j})\tilde{Z}_j(z) = T_0 e^{ibk_0} Z_0(z) +$$

$$\sum_{i=1}^{\infty} T_i e^{-bk_i} Z_i(z) \quad (x = b) \tag{25}$$

$$\sum_{j=0}^{\infty} i\tilde{k}_j \varepsilon_m(\tilde{T}_j e^{ib\tilde{k}_j} - \tilde{R}_j e^{-ib\tilde{k}_j})\tilde{Z}_j(z) = ik_0 T_0 e^{ibk_0} Z_0(z) -$$

$$\sum_{i=1}^{\infty} k_i T_i e^{-bk_i} Z_i(z) \quad (x = b) \tag{26}$$

From Eqs. (23)-(26), we notice that the left- and right-hand sides of the equations are functions of the vertical coordinate z. In order to obtain the unknown expansion coefficients, we use the orthogonality of the vertical eigenfunctions for the two-layer porous region and define an inner product as follows

$$\tilde{P}_{nl} = G_2\varepsilon_2 \int_{-H}^{-h_1-h_0} \tilde{Z}_n(z)\tilde{Z}_l(z)dz +$$

$$G_1\varepsilon_1 \int_{-h_1-h_0}^{-h_0} \tilde{Z}_n(z)\tilde{Z}_l(z)dz + \int_{-h_0}^{0} \tilde{Z}_n(z)\tilde{Z}_l(z)dz$$

$$(n,l = 0,1,2,\cdots) \tag{27}$$

In the case of $n \neq l$, we have $\tilde{P}_{nl} = 0$.

Employing the inner product on both sides of Eqs. (23)-(26) with different vertical eigenfunctions $\tilde{Z}_n(z)$ $(n = 0,1,2,\cdots)$ in the porous region, we eliminate the intermediate variables $\tilde{T}_j$ and $\tilde{R}_j$ and derive

$$I_0 e^{-ibk_0}(\tilde{k}_n Q_{0n} + k_0 P_{0n}) + R_0 e^{ibk_0}(\tilde{k}_n Q_{0n} - k_0 P_{0n}) +$$

$$\sum_{i=1}^{\infty} R_i e^{-bk_i}(\tilde{k}_n Q_{in} - ik_i P_{in}) =$$

$$T_0 e^{ib\tilde{k}_n - 2ibk_0}(\tilde{k}_n Q_{0n} + k_0 P_{0n})$$

$$\sum_{i=1}^{\infty} T_i e^{-bk_i - 2ib\tilde{k}_n}(\tilde{k}_n Q_{in} + ik_i P_{in}) \tag{28}$$

$$I_0 e^{-ibk_0}(\tilde{k}_n Q_{0n} - k_0 P_{0n}) + R_0 e^{ibk_0}(\tilde{k}_n Q_{0n} + k_0 P_{0n}) +$$

$$\sum_{i=1}^{\infty} R_i e^{-bk_i}(\tilde{k}_n Q_{in} + ik_i P_{in}) =$$

$$T_0 e^{ib\tilde{k}_n - 2ibk_0}(\tilde{k}_n Q_{0n} - k_0 P_{0n}) \cdot$$

$$\sum_{i=1}^{\infty} T_i e^{-bk_i + 2ib\tilde{k}_n}(\tilde{k}_n Q_{in} - ik_i P_{in}) \tag{29}$$

where

$$P_{nl} = G_2 \int_{-H}^{-h_1-h_0} Z_n(z)\tilde{Z}_l(z)dz + G_1 \int_{-h_1-h_0}^{-h_0} Z_n(z)\tilde{Z}_l(z)dz +$$

$$\int_{-h_0}^{0} Z_n(z)\tilde{Z}_l(z)dz \quad (n,l = 0,1,2,\cdots) \tag{30}$$

$$Q_{nl} = \varepsilon_2 \int_{-H}^{-h_1-h_0} Z_n(z)\tilde{Z}_l(z)dz + \varepsilon_1 \int_{-h_1-h_0}^{-h_0} Z_n(z)\tilde{Z}_l(z)dz +$$

$$\int_{-h_0}^{0} Z_n(z)\tilde{Z}_l(z)dz \quad (n,l = 0,1,2,\cdots) \tag{31}$$

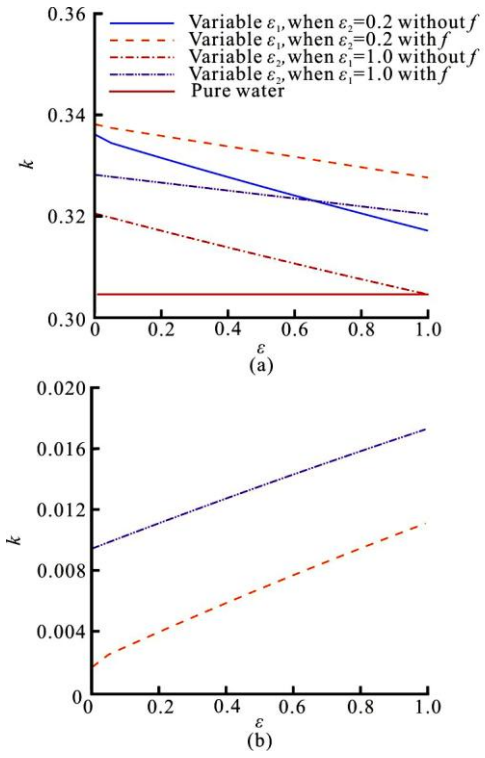

Fig. 2 (Color online) The effects of ε_1 and ε_2 on the wave numbers, where $h_0 : h_1 : h_2 = 8:1:1$, $f_1 = 1$, $f_2 = 1.3$ and $\omega = 0.3$

When we set $i = M$ from the infinite summation $\sum_i$, a combination of Eqs. (28) and (29) yields a system of $2M+2$ simultaneous equations for $2M+2$ unknown expansion coefficients, R_0, R_i,

T_0, T_i with $i=1,2,\cdots M$, which can readily be solved numerically.

3. Numerical results and discussion

For clarity, selecting two independent fundamental dimensions, the total depth of the fluid H and the gravitational acceleration g as a unit system allows us to nondimensionalize all the quantities:

$$\hat{x}=\frac{x}{H},\ \hat{z}=\frac{z}{H},\ \hat{b}=\frac{b}{H},\ \hat{h}_0=\frac{h_0}{H},\ \hat{h}_1=\frac{h_1}{H},$$

$$\hat{h}_2=\frac{h_2}{H},\ \hat{k}=kH,\ \hat{\omega}=\omega\sqrt{\frac{H}{g}},\ \hat{\zeta}_0=\frac{\zeta_0}{H},$$

$$\hat{\Phi}=\frac{\Phi}{H\sqrt{Hg}} \tag{32}$$

The nondimensional variables, throughout the rest of the paper, will be written without overhead hat symbols for convenience.

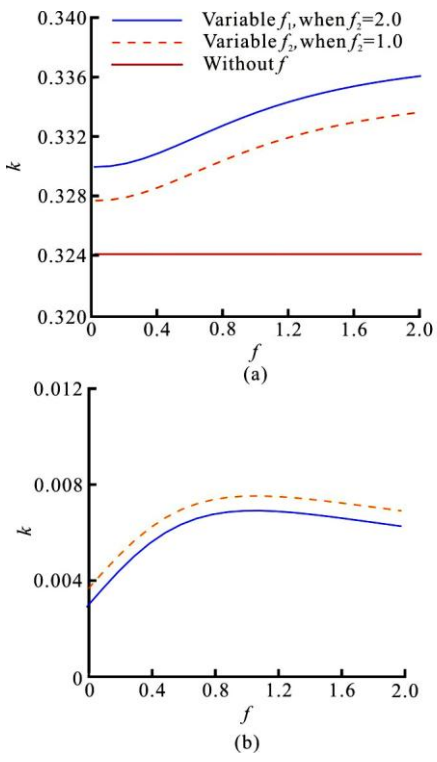

Fig. 3 (Color online) The effects of f_1 and f_2 on the wave numbers, where $h_0:h_1:h_2=8:1:1$, $\varepsilon_1=\varepsilon_2=0.4$ and $\omega=0$.

To begin with, Figs. 2-4 illustrate the effects of the parameters, which include the porosity and friction of media and the depth of the porous region, on the wave numbers (k_0 of the pure water region, $\tilde{\alpha}_0$ of the porous region and $\tilde{\beta}_0$ of the porous region). In Fig. 2, the effects of ε_1 and ε_2 on the wave numbers is shown by different lines, where $h_0:h_1:h_2=8:1:1$, $f_1=1.0$, $f_2=1.3$ and $\omega=0.3$. $\tilde{\alpha}_0$ decreases linearly and $\tilde{\beta}_0$ increases nearly linearly no matter whether ε_1 or ε_2 decreases. When $f=0$, $\tilde{\beta}_0=0$, which reveals that the amplitudes of the waves remain stable and there is no energy loss. Larger porosities result in larger wavelength and decaying rate of the waves.

Figure 3 describes the effects of f_1 and f_2 on the wave numbers, where $h_0:h_1:h_2=8:1:1$, $\varepsilon_1=\varepsilon_2=0.4$ and $\omega=0.3$. As can be seen from the figure, the values of $\tilde{\alpha}_0$ increase gradually with the increment of the friction, but the increasing relationship is nonlinear. $\tilde{\beta}_0$ reaches the peak around $f_1=1$ or $f_2=1$ and then declines slowly.

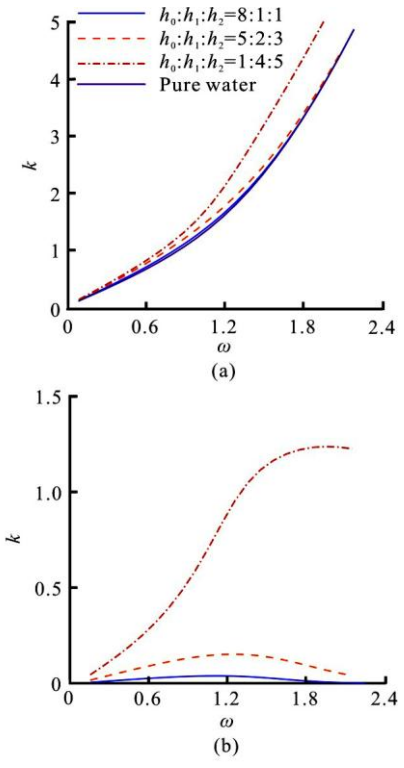

Fig. 4 (Color online) The effects of the depth rates on the wave numbers, where $\varepsilon_1=0.9$, $\varepsilon_2=0.8$ and $f_1=f_2=1.1$

The effects of the depth rates on the wave numbers are displayed in Fig. 4, where $\varepsilon_1=0.9$, $\varepsilon_2=0.8$, $f_1=f_2=1.1$ and $\omega=0.3$. The porous media occupying more region cause the curves of the

dispersion relation to move upwards. As for $\tilde{\beta}_0$, there exists a maximum point and the values of the peak become larger as the depth of the porous region increases.

For $f_1 = f_2 = 0$, we can calculate $E = (R/I_0)^2 + (T/I_0)^2 = 1$, which indicates the conservation of the energy; while for $f_1 \neq 0$ or $f_2 \neq 0$, the energy is dissipated due to the friction effect and $E = (R/I_0)^2 + (T/I_0)^2 \neq 1$. Let $E_L = |E - E_C|/E_C$ represent the relative loss of the energy, where E_C is the total energy of the reflected and transmitted waves when the computation is converged. Here we consider $h_0 = 0.5$, $h_1 = 0.3$, $h_2 = 0.2$, $\zeta_0 = 0.01$, $b = 0.4$, $\omega = 2.0$, $\varepsilon_1 = 0.9$, $\varepsilon_2 = 0.8$, $f_1 = 1.0$, $f_2 = 1.1$ and $s_1 = s_2 = 1$. Table 1 is shown to examine the convergence of the result for different M, where M is the number of evanescent modes. As M increases, the corresponding reflection $|R|$ and transmission $|T|$ coefficients converge. When $M \geq 16$, the numerical result for the energy is approximately conserved. The following figures are plotted with $M = 16$, $h_0 = 0.1$, $h_1 = 0.4$, $h_2 = 0.5$, $\zeta_0 = 0.01$ and $s_1 = s_2 = 1$ for illustration.

Table 1 The values of E and E_L for different M

M	E	E_L
2	0.917330	0.0539%
4	0.916987	0.0164%
8	0.916858	0.0024%
10	0.916847	0.0012%
12	0.916843	0.0008%
14	0.916839	0.0003%
16	0.916836	0%
18	0.916836	0%

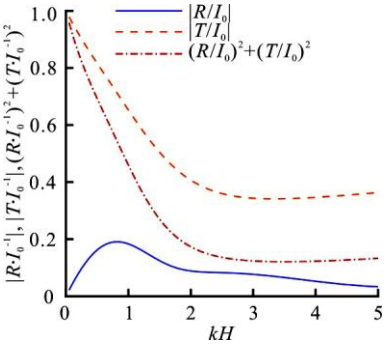

Fig. 5 (Color online) The effects of kH on the coefficients $|R/I_0|$, $|T/I_0|$ and $(R/I_0)^2 + (T/I_0)^2$, where $b = 0.4$, $\varepsilon_1 = 0.9$, $\varepsilon_2 = 0.8$, $f_1 = 1.0$ and $f_2 = 1.1$

Figure 5 shows the effects of the non-dimensional water depth kH on the coefficients $|R/I_0|$, $|T/I_0|$ and $(R/I_0)^2 + (T/I_0)^2$, where $b = 0.4$, $\varepsilon_1 = 0.9$, $\varepsilon_2 = 0.8$, $f_1 = 1.0$ and $f_2 = 1.1$. As the increment of kH, the reflection coefficients $|R/I_0|$ present a fluctuant profile and reaches the first peak at $kH \approx 0.75$, while the transmission coefficient $|T/I_0|$ firstly decreases and reaches the minimum at $kH \approx 3.5$.

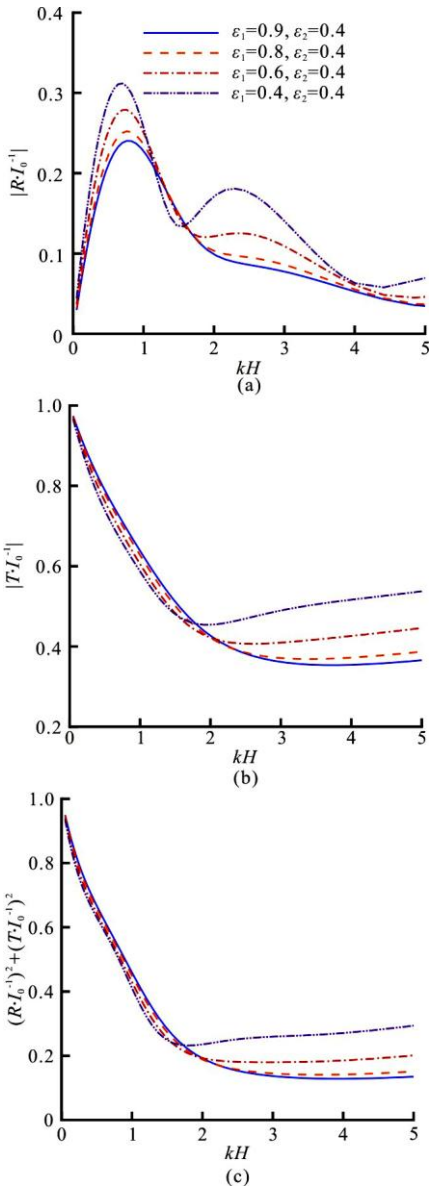

Fig. 6 (Color online) The effects of kH on the coefficients $|R/I_0|$, $|T/I_0|$ and $(R/I_0)^2 + (T/I_0)^2$ in the case of different ε_1, where $b = 0.4$, $\varepsilon_2 = 0.4$ and $f_1 = f_2 = 1$

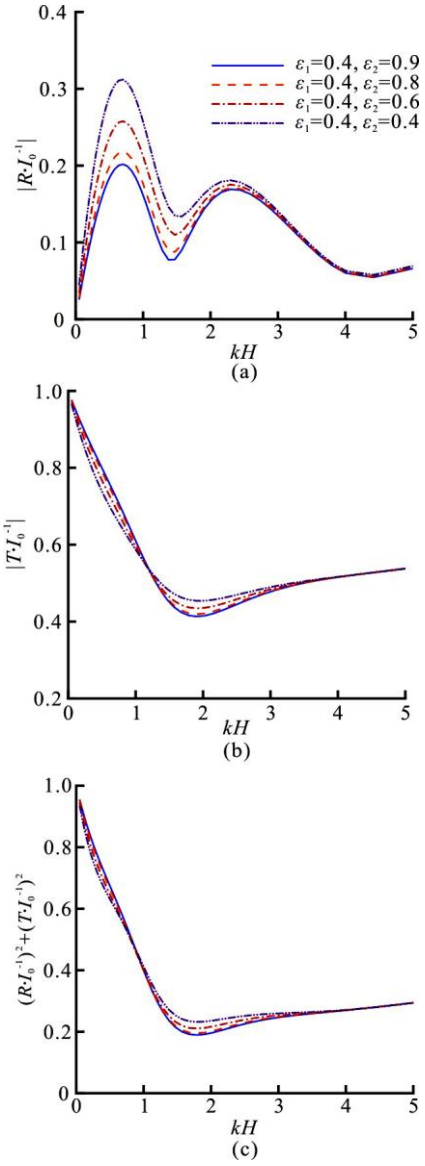

Fig. 7 (Color online) The effects of kH on the coefficients $|R/I_0|$, $|T/I_0|$ and $(R/I_0)^2+(T/I_0)^2$ in the case of different ε_2, where $b=0.4$, $\varepsilon_1=0.4$ and $f_1=f_2=1$

It is shown, in Figs. 6, 7, that the different porosities have remarkable influence on the reflection coefficients $|R/I_0|$ and the transmission coefficient $|T/I_0|$, where $b=0.4$, $f_1=f_2=1$. When ε_2 is fixed at about 0.4, the maximum of $|R/I_0|$ increases and the second peak becomes obvious as the decrease of ε_1, while the value of the transmission coefficient $|T/I_0|$ is becoming larger for larger kH. From Fig. 7, it can be seen that $|R/I_0|$ is also insensitive to the changes of ε_2, but $|T/I_0|$ is not. For $\varepsilon_1=0.4$, the smaller ε_2, the larger the peak values of $|R/I_0|$. The values of $|R/I_0|$ and $|T/I_0|$, however, remain unchanged for larger kH.

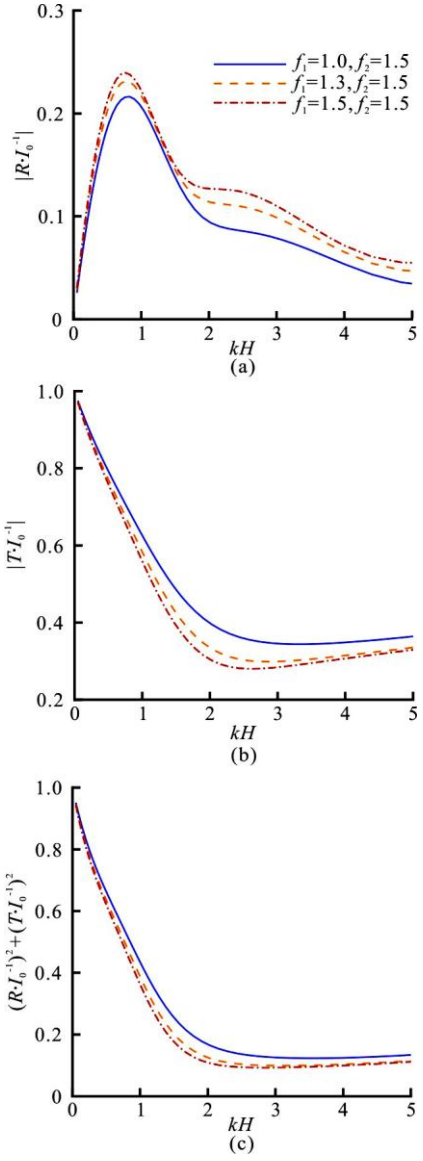

Fig. 8 (Color online) The effects of kH on the coefficients $|R/I_0|$, $|T/I_0|$ and $(R/I_0)^2+(T/I_0)^2$ in the case of different f_1, where $b=0.4$, $\varepsilon_1=0.9$ and $\varepsilon_2=0.8$

Figures 8, 9 respectively show $|R/I_0|$, $|T/I_0|$ and $(R/I_0)^2+(T/I_0)^2$ for different friction factors f_1 and f_2 of the porous region, where $b=0.4$, $\varepsilon_1=0.9$ and $\varepsilon_2=0.8$. The large friction factors enlarge the reflection coefficient $|R/I_0|$ and weaken the transmission coefficient $|T/I_0|$ due to the resistance and dissipation effects in the porous region.

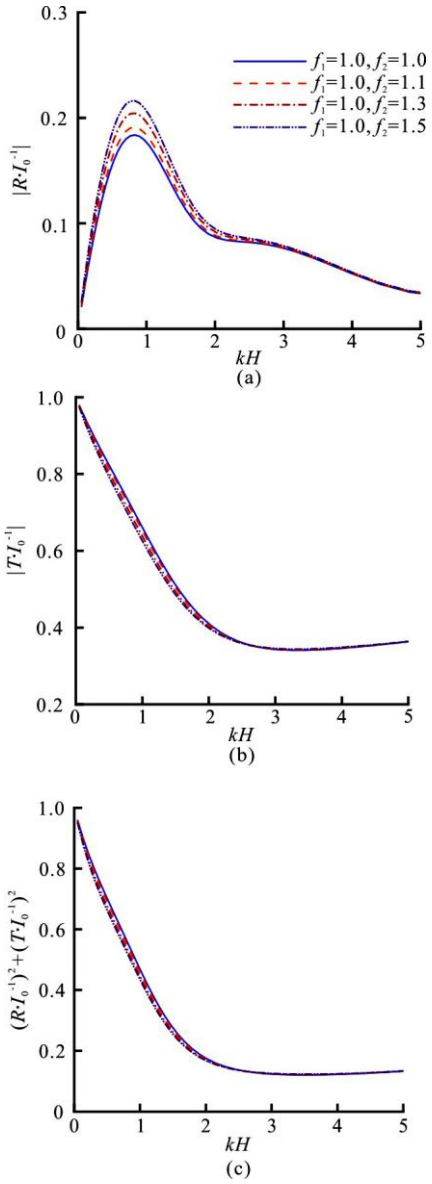

Fig. 9 (Color online) The effects of kH on the coefficients $|R/I_0|$, $|T/I_0|$ and $(R/I_0)^2+(T/I_0)^2$ in the case of different f_2, where $b=0.4$, $\varepsilon_1=0.9$ and $\varepsilon_2=0.8$

The effects of the width of the porous region on the coefficients $|R/I_0|$, $|T/I_0|$ and $(R/I_0)^2+(T/I_0)^2$ for different ε_1 and ε_2 are illustrated in Fig. 10, where $\omega=1.0$, $f_1=1.0$ and $f_2=1.1$. It is obvious that the loss of the energy increases with increasing value of b/H. The reflection coefficients $|R/I_0|$ exhibit fluctuant behavior with the increment of b/H and finally remain steady for $b/H\geq 2$. And the values of $|T/I_0|$ decline all the way back to the near-zero. Furthermore, we consider the impact of the porosity on the coefficients. The decrease of ε_1 and ε_2 will cause more reflected waves and the increase of the peak values of $|R/I_0|$. The curves with small ε_1 and ε_2 have a fast descent rate.

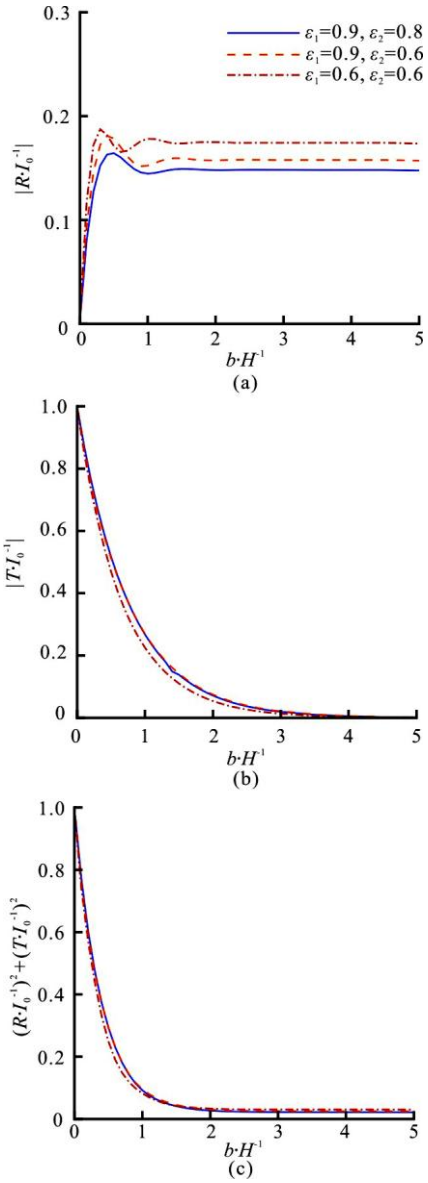

Fig. 10 (Color online) The effects of the width of b/H on the coefficients $|R/I_0|$, $|T/I_0|$ and $(R/I_0)^2+(T/I_0)^2$ in the case of different ε_1 and ε_2, where $\omega=1.0$, $f_1=1.0$ and $f_2=1.1$

4. Conclusions

This paper herein has presented an semi-analytical method for the problem that the simple time-harmonic incident waves with a given angular frequent propagate over a two-layer porous barrier. With the framework of the linear potential flow theory, we adopt the method of matched eigenfunction

expansions and define a new form of the inner product for the two-layer porous barrier to simplify the series in the simultaneous equations. A suitable truncation number of the series will save much calculating time without sacrificing the accuracy of the solution.

We have discussed the influence of the characteristics of the porous media on the dispersion relation, reflected and transmitted energy. The relationships between the wave number $\tilde{\alpha}_0$ and the porosity (ε_1 or ε_2) are linear, but the relationships between $\tilde{\alpha}_0$ and the friction (f_1 or f_2) are nonlinear. The small porosities and large friction cause the wavelength to become short. The reflection coefficients have a fluctuant profile with the increase of kH. With the decrease of the porosity ε_1 and ε_2, the reflection coefficients $|R/I_0|$ increase and the profiles exhibit fluctuant obviously, while for larger kH, the transmission coefficients $|T/I_0|$ increase to some extent. The large friction will enhance the reflection waves and reduce the transmission ones. Moreover, when the width of the porous region reaches a certain value, the reflection coefficient will remain constant, but the transmission waves will disappear.

Acknowledgements

The authors would like to thank Professor S. Q. Dai of Shanghai University for his helpful suggestions and thank the anonymous reviewers for their constructive comments.

References

[1] Sollitt C. K., Cross R. H. Wave transmission through permeable breakwaters [J]. *Coastal Engineering Proceedings*, 1972, 1(13): 1827-1846.

[2] Chwang A. T. A porous-wavemaker theory [J]. *Journal of Fluid Mechanics*, 1983, 132: 395-406.

[3] Sahoo T., Chan A. T., Chwang A. T. Scattering of oblique surface waves by permeable barriers [J]. *Journal of Waterway, Port, Coastal, and Ocean Engineering*, 2000, 126(4): 196-205.

[4] Das S., Bora S. N. Wave damping by a vertical porous structure placed near and away from a rigid vertical wall [J]. *Geophysical and Astrophysical Fluid Dynamics*, 2014, 108(2): 147-167.

[5] Zhao Y., Liu Y., Li H. J. Wave interaction with a partially reflecting vertical wall protected by a submerged porous bar [J]. *Journal of Ocean University of China*, 2016, 15(4): 619-626.

[6] Zhang J., Li Q., Ding C. et al. Experimental investigation of wave-driven pore-water pressure and wave attenuation in a sandy seabed [J]. *Advances in Mechanical Engineering*, 2016, 8(6): 1-10.

[7] Zhai Y., Zhang J., Jiang L. et al. Experimental study of wave motion and pore pressure around a submerged impermeable breakwater in a sandy seabed [J]. *International Journal of Offshore and Polar Engineering*, 2016, 28(1): 87-95.

[8] Jeng D. S. Wave dispersion equation in a porous seabed [J]. *Ocean Engineering*, 2001, 28(12): 1585-1599.

[9] Metallinos A. S., Repousis E. G., Memos C. D. Wave propagation over a submerged porous breakwater with steep slopes [J]. *Ocean Engineering*, 2016, 111: 424-438.

[10] Mohapatra S. The interaction of oblique flexural gravity incident waves with a small bottom deformation on a porous ocean-bed: Green's function approach [J]. *Journal of Marine Science and Application*, 2016, 15(2): 112-122.

[11] Das S., Behera H., Sahoo T. Flexural gravity wave motion over poroelastic bed [J]. *Wave Motion*, 2016, 63: 135-148.

[12] Shoushtari S. M. H. J., Cartwright N. Modelling the effects of porous media deformation on the propagation of water-table waves in a sandy unconfined aquifer [J]. *Hydrogeology Journal*, 2017, 25(2): 287-295.

[13] Ye J. H., Jeng D. S. Response of porous seabed to nature loadings: Waves and currents [J]. *Journal of Engineering Mechanics*, 2011, 138(6): 601-613.

[14] Zhang Y., Jeng D. S., Gao F. P. et al. An analytical solution for response of a porous seabed to combined wave and current loading [J]. *Ocean Engineering*, 2013, 57: 240-247.

[15] Zhang X., Zhang G., Xu C. Stability analysis on a porous seabed under wave and current loading [J]. *Marine Georesources and Geotechnology*, 2017, 35(5): 710-718.

[16] Seymour B. R., Jeng D. S., Hsu J. R. C. Transient soil response in a porous seabed with variable permeability [J]. *Ocean Engineering*, 1996, 23(1): 27-46.

[17] Jeng D. S., Seymour B. R. Response in seabed of finite depth with variable permeability [J]. *Journal of Geotechnical and Geoenvironmental Engineering*, 1997, 123(10): 902-911.

[18] Zhang L. L., Cheng Y., Li J. H. et al. Wave-induced oscillatory response in a randomly heterogeneous porous seabed [J]. *Ocean Engineering*, 2016, 111: 116-127.

[19] Meng Q. R., Lu D. Q. Scattering of gravity waves by a porous rectangular barrier on a seabed [J]. *Journal of Hydrodynamics*, 2016, 28(3): 519-522.